JACS
JOURNAL OF THE AMERICAN CHEMICAL SOCIETY
Article
pubs.acs.org/JACS

The Ligand Field of the Azido Ligand: Insights into Bonding Parameters and Magnetic Anisotropy in a Co(II)−Azido Complex

David Schweinfurth,[†,⊥] Michael G. Sommer,[†,⊥] Mihail Atanasov,*[,‡,§] Serhiy Demeshko,[∥] Stephan Hohloch,[†] Franc Meyer,[∥] Frank Neese,*[,‡] and Biprajit Sarkar*[,†]

[†]Institut für Chemie und Biochemie, Freie Universität Berlin, Fabeckstraße 34-36, D-14195 Berlin, Germany
[‡]Max Planck Institute for Chemical Energy Conversion, Stiftstraße 34-36, D-45470 Mülheim an der Ruhr, Germany
[§]Institute of General and Inorganic Chemistry, Bulgarian Academy of Sciences, 1113 Sofia, Bulgaria
[∥]Institut für Anorganische Chemie, Georg-August-Universität Göttingen, Tammannstraße 4, D-37077 Göttingen, Germany

Supporting Information

ABSTRACT: The azido ligand is one of the most investigated ligands in magnetochemistry. Despite its importance, not much is known about the ligand field of the azido ligand and its influence on magnetic anisotropy. Here we present the electronic structure of a novel five-coordinate Co(II)−azido complex (**1**), which has been characterized experimentally (magnetically and by electronic d−d absorption spectroscopy) and theoretically (by means of multireference electronic structure methods). Static and dynamic magnetic data on **1** have been collected, and the latter demonstrate slow relaxation of the magnetization in an applied external magnetic field of H = 3000 Oe. The zero-field splitting parameters deduced from static susceptibility and magnetizations (D = −10.7 cm^{-1}, E/D = 0.22) are in excellent agreement with the value of D inferred from an Arrhenius plot of the magnetic relaxation time versus the temperature. Application of the so-called *N*-electron valence second-order perturbation theory (NEVPT2) resulted in excellent agreement between experimental and computed energies of low-lying d−d transitions. Calculations were performed on **1** and a related four-coordinate Co(II)−azido complex lacking a fifth axial ligand (**2**). On the basis of these results and contrary to previous suggestions, the N_3^- ligand is shown to behave as a strong σ and π donor. Magnetostructural correlations show a strong increase in the negative D with increasing Lewis basicity (shortening of the Co−N bond distances) of the axial ligand on the N_3^- site. The effect on the change in sign of D in going from four-coordinate Co(II) (positive D) to five-coordinate Co(II) (negative D) is discussed in the light of the bonding scheme derived from ligand field analysis of the ab initio results.

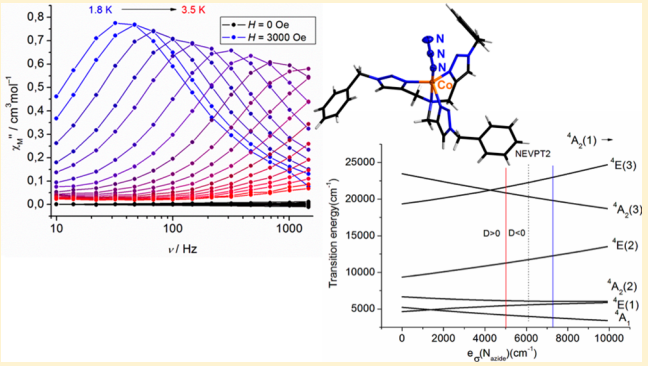

INTRODUCTION

Except for a series of pseudotetrahedral complexes of Co^{II} [supported by the hydrotris(3-R,5-R′-pyrazol-1-yl)borate ("scorpionate") anion (Tp$^{R,R'}$) with equatorial N pyrazole donors and variable axial ligands L = Cl$^-$, NCS$^-$, NCO$^-$, and N_3^- (**2**)],[1] little is known about the ligand field of the azido (N_3^-) ligand and its influence on optical d−d absorption spectra and the magnetic anisotropy in axial and orthorhombic complexes of the late 3d transition metals. This series of complexes has been studied by high-field electron paramagnetic resonance (EPR) and electronic absorption spectroscopy.[1] By means of the angular overlap model (AOM), Co−L bonding parameters were deduced from best fits of optical d−d absorption and high-field EPR spectra. In these interpretations, to account for the known circumstance that AOM parameters in complexes with geometries close to cubic (tetrahedral and octahedral) cannot be uniquely determined from a best fit of optical spectra, π Co−ligand donor functions[1] were neglected (i.e., the corresponding energy parameters e_π were set to zero). In contrast to the complex of the present study, the zero-field splitting (ZFS) parameter D in the entire series deduced from high-field EPR spectra was reported to be positive. Interestingly enough, the N_3^- ligand was shown to act as bridging ligand in the Mn^{III}-based nanomagnets [Mn_3Zn_2] with planar [$Mn_3^{III}(\mu_3$-oxo)]$^{7+}$ cores.[2] The azido ligand has found widespread use in magnetochemistry and is known to take up various coordination modes.[3] Hence, an understanding of the ligand field properties of the azido ligand is relevant for many different fields in magnetism.

Here we report the synthesis and magnetic and spectroscopic characterization of the novel complex [Co^{II}(tbta)N_3]$^+$ (**1**) (tbta = tris[(1-benzyl-1*H*-1,2,3-triazol-4-yl)methyl]amine), which exhibits slow relaxation of the magnetization in an external magnetic field. Click-derived ligands are currently immensely popular in coordination and organometallic chemistry,[4] and

Received: November 30, 2014
Published: January 14, 2015

DOI: 10.1021/ja512232f
J. Am. Chem. Soc. 2015, 137, 1993−2005

tbta has been the most extensively studied click-derived tripodal ligand for metal coordination.[5] The electronic structure of **1** has been studied here experimentally by means of d−d absorption spectra and magnetometry and theoretically by multireference electronic structure calculations. Analysis of the theoretical results using a recently developed ab initio-based ligand field theory[6−8] allowed the extraction of ligand field orbital splitting diagrams, which were further used to deduce bonding parameters for the different ligands of the coordination sphere of Co^{II}. With these parameters in hand, magnetostructural correlations were derived. These allowed us to deduce the effect of the coordination number, the complex geometry, and the Lewis basicity of the axial ligand on the magnetic anisotropy, i.e., the sign and magnitude of the ZFS parameter *D*.

EXPERIMENTAL SECTION

General Considerations. All of the chemicals were commercially available and used as received without further purification, unless otherwise stated. Solvents for synthesis were dried prior to use with appropriate drying agents. All of the manipulations were carried out under an inert atmosphere of nitrogen using standard Schlenk techniques. Tbta was synthesized according to a literature procedure.[9] Elemental analysis (CHN) was measured with Elementar Vario EL III and PerkinElmer model 240 analyzers. Attenuated total reflectance Fourier transform IR (ATR-FTIR) spectra were recorded with a Thermo Scientific Nicolet iS10 FTIR spectrometer equipped with a smart orbit unit. Mass spectrometry was run on an Agilent 6210 ESI-TOF instrument (Agilent Technologies, Santa Clara, CA, USA). UV−vis spectra were recorded with an Avantes spectrometer consisting of a light source (AvaLight-DH-S-Bal), a UV−vis detector (AvaSpec-ULS2048), and a near-IR (NIR) detector (AvaSpec-NIR256-TEC).

Synthesis of [Co(tbta)N_3]ClO_4·3CH_3CN (1). $Co(ClO_4)_2·6H_2O$ (129 mg, 0.353 mmol), tbta (187 mg, 0.353 mmol), and $[NBu_4]N_3$ (100 mg, 0.353 mmol) were dissolved in CH_3CN (10 mL), and the solution was stirred at room temperature for 16 h. The purple reaction solution was filtered, and Et_2O was evaporated into the filtrate. $[Co(tbta)N_3]ClO_4·3CH_3CN$ was isolated by filtration as purple crystals (220 mg, 73%) suitable for X-ray crystallography. Anal. Calcd for $C_{36}H_{39}ClCoN_{16}O_4$: C, 50.62; N, 26.24; H, 4.60. Found: C, 50.71; N, 26.21; H, 4.61. IR (azide): 2077 cm^{-1}. HRMS (ESI): calcd for $C_{30}H_{30}N_{13}Co$, 631.2079; found, 631.1965.

Caution! *Although we never experienced any problems, azide and perchlorate salts are potentially explosive and should be handled with great care.*

Computational Details. The d^7 configuration of Co^{II} gives rise to 10 $S = {}^3/_2$ and 40 $S = {}^1/_2$ electronic multiplets. Nonrelativistic energy levels and wave functions were computed using the complete-active-space self-consistent field (CASSCF) method,[10] averaging over the electron densities of all considered states and taking an active space with seven electrons distributed over the five 3d molecular orbitals (MOs) [CAS(7,5)]. To study the effect of electrons on bonding orbitals dominated by bonding ligand orbitals, a refined calculation was done in which the active space was extended to include the doubly occupied σ and π orbitals of the N donor of the N_3^- ligand. In CASSCF, static correlation (near degeneracy) is taken into account, so in a sense, CAS(7,5) calculations can be qualified as an ab initio-based crystal field theory. Depending on the chosen active space, dynamical (short-range) correlation is partly or completely ignored in such a treatment. To account for dynamical correlation, *N*-electron valence perturbation theory to second order (NEVPT2)[11−15] was the method of choice. The effect of NEVPT2 is to replace the diagonal matrix elements of the configuration interaction (CI) matrix given by CASSCF with improved diagonal energies. Such a replacement provides more accurate (but still approximate) energetics while keeping the same (zeroth-order) CASSCF wave function. CASSCF and NEVPT2 methods have been efficiently implemented in the program ORCA[16,17] and allow computations on real systems (without the necessity of model truncations) with unprecedented size (up to 100−200 atoms and 2000 contracted basis functions). From the resulting energies of many-electron states, magnetic properties were computed by applying a computational protocol described elsewhere.[7] To this end, spin−orbit coupling (SOC) was taken into account using a mean-field SOC operator.[18,19] Mixing of nonrelativistic CI eigenfunctions and splitting of the corresponding eigenvalues were taken into account using quasi-degenerate perturbation theory (QDPT).[19]

To extract orbital energies and bonding parameters from the correlated calculations, we applied a one-to-one mapping of the Hamiltonian CI matrix $\mathbf{H}_{CI}$ onto the same matrix expressed in terms of ligand field parameters p_i (eq 1):

$$\mathbf{H}_{CI} = \sum_i p_i \mathbf{H}_i \tag{1}$$

where the $\mathbf{H}_i$ are coefficient matrices (see refs 6 and 8 for more details). This results in an overdetermined system of linear equations for the unknown parameter vector $\mathbf{P} = \{p_1, p_2, ..., p_n\}$ (eq 2):

$$\mathbf{AP} = \mathbf{Y} \tag{2}$$

The parameter vector **P** was then determined by least-squares according to eq 3:

$$\mathbf{P} = (\mathbf{A}^T\mathbf{A})^{-1}\mathbf{A}^T\mathbf{Y} \tag{3}$$

Here we confined the computations to the manifold of the 10 $S = {}^3/_2$ states, which were used to deduce the symmetric 5 × 5 one-electron ligand field matrix $\mathbf{V}_{LF}$ (defined by 15 independent matrix elements) and one parameter of interelectronic repulsion, *B*. Diagonalization of $\mathbf{V}_{LF}$ yielded one-electron ligand field energy diagrams. More detailed information about the Co−N bond was extracted from $\mathbf{V}_{LF}$ by employing the angular overlap model.[20,21] In this model, metal−ligand antibonding energies of σ (e_σ) and π (e_π) type are defined using optimally aligned metal−ligand d_{z^2}−p_z and (d_{xz}−p_x, d_{yz}−p_y) orbitals, respectively. The matrix elements of $\mathbf{V}_{LF}$ are then expressed in terms of such parameters times angular factors that account for the ligand positions. To this end, we utilized the geometries of **1** and **2** from X-ray data and (for **1**) also a density functional theory (DFT)-optimized geometry (with van der Waals corrections for nonbonding interactions included, following ref 22). In these as well as in the correlated calculations, triple-ζ valence quality basis sets (def2-TZVP)[23,24] were used. Environmental effects were included using the conductor-like screening model (COSMO).[25,26] Linear expressions for the ligand field Hamiltonian in terms of the parameters **P** were derived using the program AOMX.[27]

X-ray Crystallography. Single-crystal X-ray diffraction data were collected with a Bruker AXS Smart diffractometer. Data were collected at 100(2) K using graphite-monochromatized Mo Kα radiation (λ = 0.71073 Å). The strategy for the data collection was evaluated using the Smart software. The data were collected by standard ψ−ω scan techniques and scaled and reduced using Saint+ software. The structures were solved by direct methods using SHELXS-97 and refined by full-matrix least-squares with SHELXL-97, refining on F^2.[28] The positions of all of the atoms were obtained by direct methods. All non-hydrogen atoms were refined anisotropically. The remaining hydrogen atoms were placed in geometrically constrained positions and refined with isotropic temperature factors, generally 1.2 times the U_{eq} values of their parent atoms. CCDC 966778 contains the crystallographic information for $[Co(tbta)N_3]ClO_4·3CH_3CN$.

Magnetic Measurements. Magnetic susceptibility measurements were carried out with a Quantum Design MPMS-XL-5 SQUID magnetometer. The powdered sample was contained in a gel bucket, covered with a few drops of low-viscosity inert oil to avoid orientation of the crystals in the magnetic field, and fixed in a nonmagnetic sample holder. Each raw data file for the measured magnetic moment was corrected for the diamagnetic contributions of the gel bucket and the oil using experimentally obtained gram susceptibilities for the gel bucket and the oil. The molar susceptibility data were corrected for the diamagnetic contribution according to $\chi_M^{dia}(\text{sample}) = -0.5M \times 10^{-6}$ $cm^3·mol^{-1}$, where *M* is the molecular weight.[29] Temperature-

DOI: 10.1021/ja512232f
J. Am. Chem. Soc. 2015, 137, 1993−2005

independent paramagnetism (TIP) was included according to the expression $\chi_{calc} = \chi + TIP$, where TIP = 450 × 10^{-6} cm^3 mol^{-1} for **1**.

RESULTS AND DISCUSSION

Synthesis and Coordination Geometries. Complex **1** was synthesized in a one-pot reaction of $Co(ClO_4)_2 \cdot 6H_2O$, tbta, and $[NBu_4]N_3$ as an azide source. Filtration of the reaction mixture and crystallization of the filtrate led to the isolation of purple single crystals that were used for structure determination as well as for the magnetic measurements. **1** crystallizes in the triclinic $P\bar{1}$ space group as an acetonitrile solvate. The geometry of Co^{II} in **1** can be roughly described as a distorted CoN_5 trigonal bipyramid (Figure 1) with one long axial bond to a tertiary amine nitrogen (Co−N_{amine}, 2.369 Å) and, trans to it, a short one to the azide nitrogen (Co−N_{azide}, 1.964 Å) (Table 1). Nitrogen donors from the triazole rings of the tbta ligand complete the trigonal plane, with Co−N_{tbta} distances that are intermediate between the above two (2.035 Å). There is a considerable shift of Co^{II} out of the $(N_{tbta})_3$ plane, with N_{azide}−Co−N_{tbta} and N_{amine}−Co−N_{tbta} angles considerably larger and smaller than 90°, respectively. The linear free N_3^- in the given complex coordinates in a nonlinear fashion to Co with a Co−N_{azide}−N'_{azide} angle of 141.13°. In Figure 2 we compare the N−N bond lengths within the ligand (Table 1) with the ones reported for free N_3^- and the acid N_3H as well as with standard N−N, N=N, and N≡N bond lengths. The comparison shows that upon complex formation the N_3^- ligand undergoes minor changes and approaches a geometric structure with N−N bond distances characteristic of a nitrogen−nitrogen double bond and (in contrast to N_3H) quite similar to those of the free N_3^- ion. The bond distances and angles from a DFT geometry optimization (Table 1) compare well with the experimental ones. It is worth comparing the geometry of five-coordinate **1** with that of the pseudotetrahedral complex **2** without a ligand trans to the Co−N_3 bond.[1] As will be shown here, this difference in the structures of complexes **1** and **2** has crucial consequences for their electronic structures and magnetic anisotropy. On the basis of a comparison between bond distances and bond angles of **1** and **2**, we can conclude that the coordination modes of the tbta, $Tb^{3\text{-t-Bu}}$, and N_3^- ligands are quite similar. The lack of a fifth ligand trans to the Co−N_{azide} bond in **2** correlates with a distinctly shorter Co−N_{azide} bond length than the one reported in **1**.

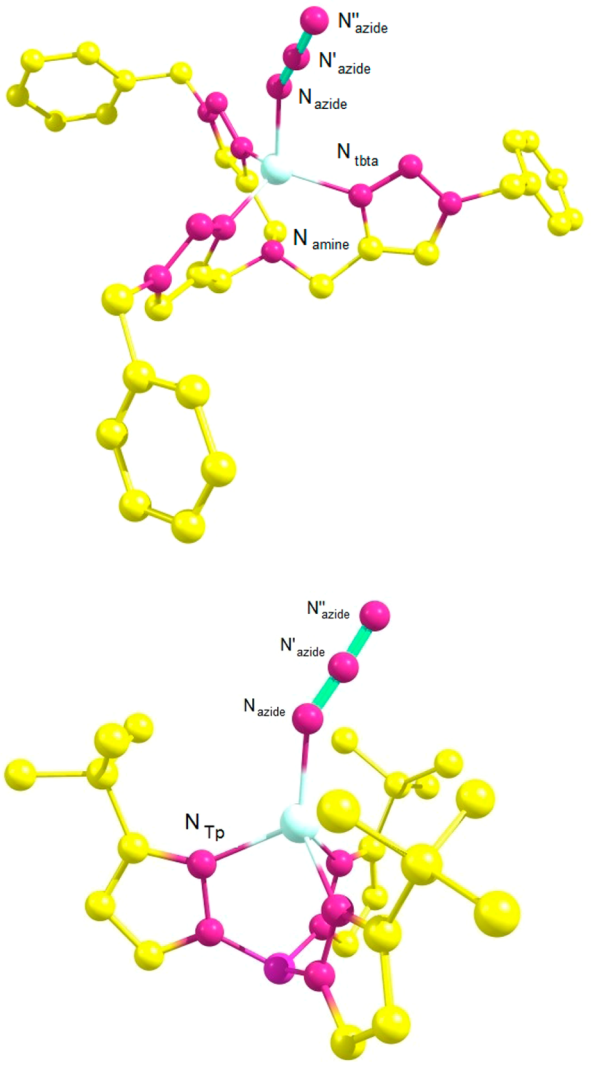

Figure 1. Geometries of (top) $[Co^{II}(tbta)N_3]^+$ (**1**) and (bottom) $[Co^{II}(Tp^{3\text{-t-Bu}})N_3]$ (**2**)[1] as given by the X-ray structures of $[Co^{II}(tbta)N_3](ClO_4)\cdot 3CH_3CN$ and $[Co^{II}(Tp^{3\text{-t-Bu}})N_3]$, respectively. Color code: Co, light green; N, magenta; C, yellow; B, violet. Notations for the N atoms coordinated to Co^{II} used in the definition of the bond distances and bond angles in Table 1 are listed.

Static and Dynamic Magnetic Properties. The direct current (dc) magnetic susceptibility of **1** was measured as a function of the temperature between 2.0 and 215 K (H = 0.5 T), and the results are shown in Figure 3 as a plot of $\chi_M T$ versus T. $\chi_M T$ saturates at a value of 2.57 cm^3 K mol^{-1} for T above 50 K and is consistent with a $S = {}^3/_2$ spin ground state and Curie−law behavior. From eq 4 an effective g tensor (g_{eff}) value of 2.34 was deduced, showing the expected orbital contributions to the spin-only value (g_0 = 2.0023).

$$\chi_M T = \left(\frac{N_A \mu_B^{\,2}}{3k_B}\right) g_{eff}^{\,2} S(S+1) = 0.125 g_{eff}^{\,2} S(S+1) \tag{4}$$

Below 50 K, $\chi_M T$ shows a sharp drop, which because of the large separation between neighboring CoN_5 units [the shortest Co−Co distance is 8.186(1) Å] is interpreted as a hallmark of a significant zero-field splitting (magnetic anisotropy). From a fit of the $\chi_M T$ data to the spin Hamiltonian in eq 5 (in this fit the orthorhombic ZFS parameter E was set to zero), the values g_{eff} = 2.34 and $|D|$ = 11.3 cm^{-1} were obtained.

$$\begin{aligned}\hat{H}_{SH} &= \hat{H}_{ZFS} + \hat{H}_{Zeeman} \\ &= D[\hat{S}_z^{\,2} - S(S+1)/3] + E(\hat{S}_x^{\,2} - \hat{S}_y^{\,2}) + g_{eff}\mu_B \mathbf{H}\cdot\hat{\mathbf{S}}\end{aligned} \tag{5}$$

The field dependence of the magnetization M_{mol} was studied over the temperature range 1.8−100 K and at field values of H = 1, 3, and 5 T (Figure 4). The nesting of the sets of data for different fields is in support of the magnetic anisotropy, and a fit of the data with the Hamiltonian of eq 5 (Figure 4, solid lines) yielded the value $|D|$ = 10.7 cm^{-1}, in agreement with the one resulting from the fit to the $\chi_M T$ data. In addition, the fit yielded a large orthorhombic parameter E (E/D = 0.22; in these simulations, the value of g_{eff} was fixed at 2.34). It should be noted that the sign of D cannot be reliably determined from simulations of $\chi_M T$ and M_{mol}. Theoretical results unambiguously showed that D is negative (see below). A reasonably large and negative D leads one to expect that **1** might behave as a

DOI: 10.1021/ja512232f
J. Am. Chem. Soc. 2015, 137, 1993−2005

Table 1. Structural Parameters of $[Co^{II}(tbta)N_3]^+$ (Pseudo-Trigonal-Bipyramidal, from X-ray Data and DFT Geometry Optimization) and $[Co^{II}(Tp^{3\text{-}t\text{-}Bu})N_3]$ (Pseudotetrahedral, from X-ray Data)

	$[Co^{II}(tbta)N_3]^+$		$[Co^{II}(Tp^{3\text{-}t\text{-}Bu})N_3]$
	X-ray (SMM)	DFT-optimized[a]	X-ray
	Bond Distances (Å)		
$Co-N_{azide}$	1.964(3)	1.937	1.919
$Co-(N_{tbta}/N_{Tp})$	2.032(3)	2.013	2.035
	2.032(3)	2.010	2.032
	2.042(3)	2.008	2.035
$Co-N_{amine}$	2.369(3)	2.462	–[b]
$N_{azide}-N'_{azide}$	1.169	1.204	1.178
$N'_{azide}-N''_{azide}$	1.161	1.166	1.156
	Bond Angles (deg)		
$N_{azide}-Co-(N_{tbta}/N_{Tp})$	106.28(11)	103.71	122.47
	100.16(11)	108.70	124.39
	109.92(12)	106.39	117.90
$N_{amine}-Co-N_{tbta}$	78.01(10)	73.75	–
	74.57(10)	73.82	–
	73.90(10)	73.59	–
$(N_{tbta}/N_{Tp})-Co-(N_{tbta}/N_{Tp})$	113.42(11)	111.90	95.16
	112.47(11)	112.61	95.87
	113.42(11)	112.88	94.12
$Co-N_{azide}-N'_{azide}$	141.13(11)	128.78	139.96
$N_{azide}-N'_{azide}-N''_{azide}$	176.23(11)	177.24	176.79
$N_{azide}-Co-N_{amine}$	173.80(11)	177.15	–

[a]Cartesian coordinates for the DFT-optimized geometry are listed in the Supporting Information. [b]Co–B distance of 2.945 Å.

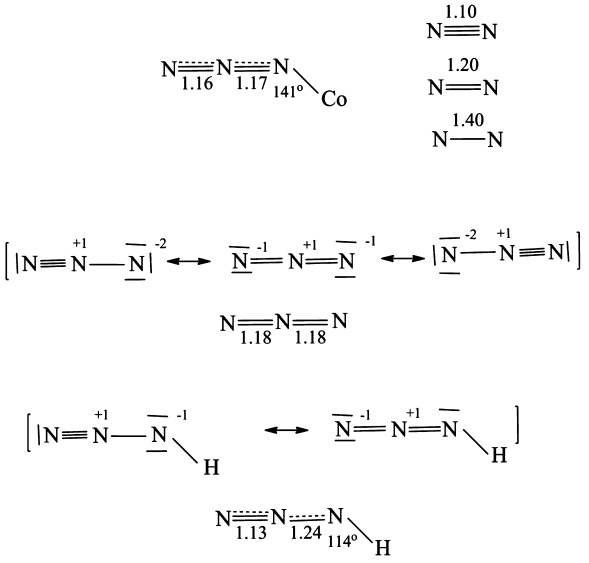

Figure 2. Resonance structures of the free and coordinated N_3^- ligand and correlations of the N–N bond lengths within the ligand in its free and coordinated forms as well as standard N–N, N=N, and N≡N bond lengths.

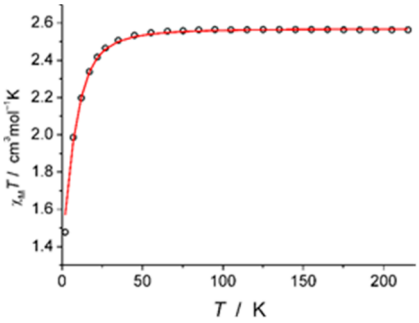

Figure 3. Temperature dependence of the static magnetic susceptibility of **1** (H = 0.5 T, open black circles) and its simulation in terms of the spin Hamiltonian in eq 5 (solid red line). The best-fit parameters are $|D|$ = 11.3 cm^{-1} and g_{eff} = 2.34. The experimental data were corrected for TIP (χ_{TIP} = 450 × 10^{-6} $cm^3 \cdot mol^{-1}$).

single-molecule magnet, and indeed, alternating current (ac) magnetic susceptibility data collected in a field H_{dc} = 3000 Oe displayed temperature- and frequency-dependent maxima in the out-of-phase ac susceptibility (χ''_M) (Figure 5, top). This indicates slow relaxation of the magnetic moment over the accessible frequency (ν) and temperature ranges (T was varied between 1.8 and 3.5 K in steps of 0.1 K). The maximum of the χ''_M versus ν curve shifted to larger ν with increasing temperature and above T = 2.5 K was outside of the accessible frequency range. From the linear region of the Arrhenius plot of the magnetic relaxation time [$\ln(\tau) = \ln(1/\nu_{max})$ vs $1/T$; Figure 5, bottom], comprising the four higher values of T (2.5, 2.4, 2.3, and 2.2 K), values of the spin-reversal barrier (U_{eff} = $-2D$ = 19.7 cm^{-1}) and the attempt time (τ_o = 1.60 × 10^{-8} s) were deduced. The value of D extracted in this way ($D = U_{eff}/2$ = −9.9 cm^{-1}) closely matches the one deduced independently from the static $\chi_M T$ and M_{mol} data (see above). The τ_o value of 1.60 × 10^{-8} s is within the range typically observed for single-molecule magnets.[30] The deviations from the straight line at lower temperatures (T = 2.1–1.8 K) reflect the shortcut of the relaxation time due to the onset of quantum tunneling of the magnetization. Such tunneling and the absence of a maximum in the χ''_M versus ν curves in the absence of an external magnetic field (Figure 5, top) are consistent with the structure of **1** showing a large orthorhombic component. This causes an off-axial ligand field and leads to transversal magnetic anisotropy, reflected by the ZFS parameter E deduced from the static magnetic data. **1** thus is the first example of a mononuclear

DOI: 10.1021/ja512232f
J. Am. Chem. Soc. 2015, 137, 1993–2005

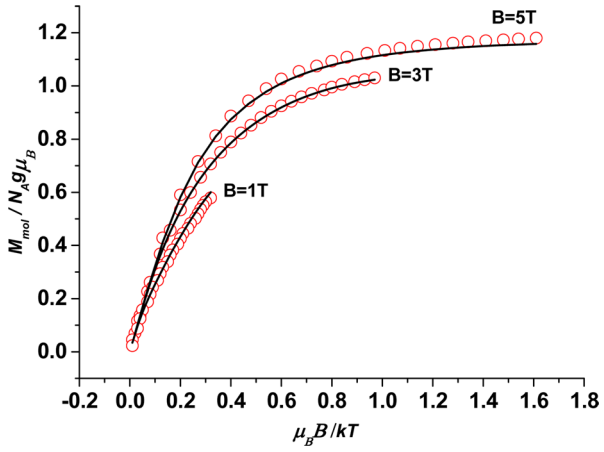

Figure 4. Field dependence of the magnetization of **1** and its simulation (solid lines). The best-fit parameters are $|D| = 10.7$ cm^{-1} and $E/D = 0.22$ (in the simulations, g_{eff} was fixed at the value resulting from the best fit of the magnetic susceptibility; see Figure 3).

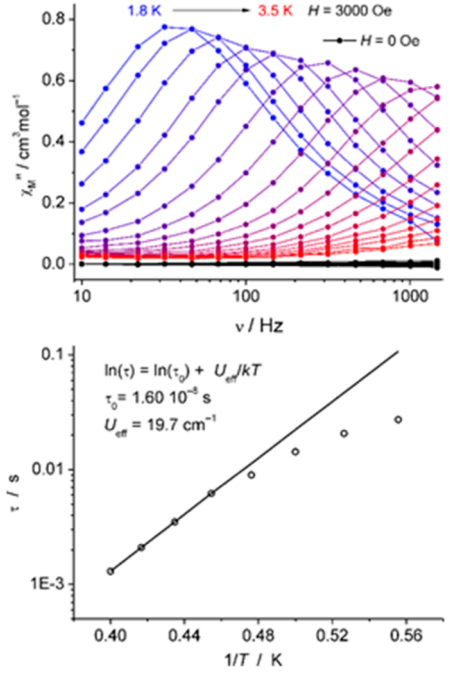

Figure 5. (top) Frequency dependence of the imaginary part of the alternating current susceptibility χ_M'' without a dc field (black symbols) and with H_{dc} = 3000 Oe (symbols from blue to red). (bottom) Arrhenius plot of the temperature dependence of the relaxation time τ. The black straight line describes thermally activated (Orbach) relaxation, which dominates at the four higher temperatures (T = 2.5, 2.4, 2.3, and 2.2 K).

Co(II) complex containing the magnetically ubiquitous N_3^- ligand that displays single-molecule magnet behavior.

d−d Absorption Spectra. The electronic absorption spectrum of **1** (Figure 6, top) displays absorption bands of low intensity extending from the NIR to the visible region (up to 23000 cm^{-1}) and intense charge transfer (CT) transitions in the upper energy range. On the basis of CASSCF/NEVPT2 calculations, spin-allowed d−d transitions were predicted to take place from the $^4A_2(1)$ ground state into the $^4A_1$, $^4E(1)$, $^4A_2(2)$, $^4E(2)$, $^4A_2(3)$, and $^4E(3)$ excited states in increasing order of energy (Tables 2 and 3; notations of energy levels are

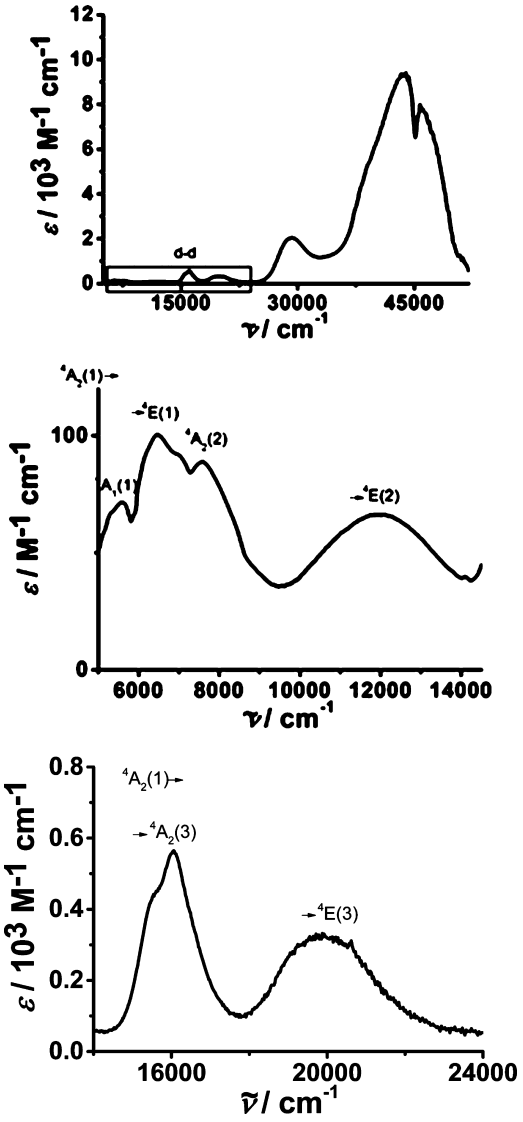

Figure 6. (top) Electronic absorption spectrum of **1**, with the spectral region dominated by d−d transitions highlighted. (middle) NIR spectral region. (bottom) Visible spectral region. Assignments of band maxima and shoulders to the spin-allowed transitions from the $^4A_2$ ground state to the ^4E and $^4A_2$ excited states are given within the C_{3v} pseudosymmetry of the complex.

given according to the irreducible representations of the C_{3v} point group). As depicted in Figure 6, it was possible to identify *all of the d−d transitions* in the spectrum. A comparison between the d−d band maxima in the NIR region and the computed term energies originating from the ^4F term of the free Co^{2+} ion (Tables 2 and 3) shows good agreement between theory and experiment, in particular when dynamical correlation was taken into account (NEVPT2 results). In contrast, excited electronic terms split out from the ^4P term of the free Co^{2+} ion were computed to be 3675−5840 cm^{-1} higher in energy than experiment. The reason for this is the proximity of these states to higher-lying CT states (Figure 6, top). The influence of these CT states was excluded when the active space with seven d electrons correlated on five d orbitals [CAS(7,5)] was chosen. The effect of CT states is not only to mix into the 3d multiplets, shifting these to lower energies, but also to increase the intensities of the respective d−d transitions. Computations based on the CASSCF wave functions under-

DOI: 10.1021/ja512232f
J. Am. Chem. Soc. 2015, 137, 1993−2005

Table 2. Energies (ΔE in cm^{-1}) and Oscillator Strengths (f) of Electronic Transitions from the $^4A_2(1)$ Ground State to the Indicated States As Obtained by CASSCF/NEVPT2 Calculations and Deduced from Deconvolution of the Band Profile of the Solution Absorption Spectrum of $[Co^{II}(tbta)N_3](ClO_4)$

	CASSCF		NEVPT2		experimental[a]		
state[b]	ΔE	$10^5 f$	ΔE	$10^5 f$	b_1	$\varepsilon_{exptl}(b_3)$	$10^5 f_{exptl}$
$^4A_1(1)$	3718	0.11	4986	0.14	5430	33	12.3
$^4E(1)$	5120	1.47	6649	1.91	6200	42	4.1
	5324	1.94	6877	2.51	6590	42	25.6
$^4A_2(2)$	6181	5.02	8064	6.55	7740	39	30.3
$^4E(2)$	10321	1.71	13457	2.24	11960	32	37.1
	10331	1.58	13466	2.06			
$^4A_2(3)$	22490	39.79	21140	37.40	15300	398	21.0
					16030	171	239.9
$^4E(3)$	24616	12.59	23615	12.08	19940	279	339.8
	24845	12.26	24002	11.84			

[a]Based on the deconvolution of the d−d absorption spectrum into Gaussian components $b_3 \exp[(x - b_1)^2/b_2^2]$. Values of b_1 (in cm^{-1}) are compared with the energies of d−d transitions from the CASSCF/NEVPT2 calculations. The values of b_2 (in cm^{-1}) and b_3 pertaining to the entries in the last column are (from top to bottom) 486, 33; 279, 19; 618, 54; 789, 50; 1511, 32; 297, 92; 801, 478; 1652, 268. For the sake of comparison between theoretical and experimental oscillator strengths f, values of f_{exptl} were estimated using the equation $f = (4.61 \times 10^{-9})\varepsilon_{max}\tilde{\nu}_{1/2}$, in which $\tilde{\nu}_{1/2}$ is the full width at half-maximum ($\varepsilon_{max}/2$): $\tilde{\nu}_{1/2} = 2(\ln 2)^{1/2} b_2 b_3$. [b]Term notations correspond to the irreducible representations of the C_{3v} pseudosymmetry.

Table 3. Effect of the Extension from the d-Only Active Space [CAS(7,5)] to Active Spaces Including Two π [CAS(11,7)] or Two π and One σ [CAS(13,8)] Doubly Occupied MOs Dominated by Azide N-Donor Orbitals, State-Averaged over All of the $S = {}^3/_2$ States (SA) or State-Specific (SS) Where Averaging Was Done within the Three Topmost 3d Terms $^4A_2(3)$ and $^4E(3)$[a]

	CAS(7,5), SA	CAS(11,7), SA	CAS(13,8), SA	CAS(13,8), SS	exptl
$^4A_2(1) \rightarrow {}^4A_2(3)$	21140 (5475)	20660 (4995)	20620 (4955)	19623 (3958)	15665[c]
$^4A_2(1) \rightarrow {}^4E(3)$[b]	23808 (3868)	23236 (3296)	23200 (3260)	22177 (2237)	19940

[a]Only NEVPT2 results are listed; differences between the computed and experimental values are listed in parentheses. [b]Averaged over the two components split in low symmetry: 23615, 24002; 23060, 23412; 23024, 23377; 22004, 22350 cm^{-1}. [c]Averaged over the doublet structure with energies deduced from a Gaussian deconvolution: 15300, 16030 cm^{-1}.

estimated these intensities by more than one order of magnitude (Table 2). However, extending the active space to include electrons in σ and π MOs on N_3^- lowered the energies of the $^4A_2(3)$ and $^4E(3)$ states and thus improved the agreement with the experimentally observed transitions (Table 3).

The polarized electronic spectrum of $[Co(NCS)(Me_6tren)](SCN)$, a $Co^{II}N_5$ complex with a geometry similar to that of **1** but different N donors, has been reported elsewhere.[31] The energies of the d−d transitions and their assignments based on the observed polarizations ratios and a ligand field analysis show a similar energy level ordering as for **1** but quite different term energetics: 5800 cm^{-1} [$^4A_2(1) \rightarrow {}^4E(1)$], 14800 cm^{-1} [$^4A_2(1) \rightarrow {}^4E(2)$], 16500 cm^{-1} [$^4A_2(1) \rightarrow {}^4A_2(3)$], 21000 [$^4A_2(1) \rightarrow {}^4E(3)$]). However, in contrast to the complex reported here, the variation of the ligand field due to the difference of the involved N-donor ligands did not allow detection of the energies of the two lowest transitions, $^4A_2(1) \rightarrow {}^4A_1(1)$ and $^4A_2(1) \rightarrow {}^4A_2(2)$.

One can conclude from the observed and computed d−d transitions that the electronic structure of **1** is dominated by the trigonal ligand field, which leads to a large magnetic anisotropy as reflected by the ZFS parameter D (see above). However, as manifested by the structural angles of the complex (Table 1), the observed and computed sublevels of the $^4E(1)$ state display in addition a significant orthorhombic splitting. As shown in Theoretical Analysis (see below), this orthorhombic anisotropy is the cause of the comparably large values of the ZFS parameter E.

It is instructive to compare the level ordering deduced from the spectra of **1** with that of the four-coordinate Co^{II} complex **2**, which lacks a fifth ligand trans to the Co−N_3 bond[1] but otherwise displays an angular geometry and ligands similar to those of **1**. Here electronic transitions from the $^4A_2(^4F)$ ground state into the $^4T_2(^4F)$, $^4T_1(^4F)$, and $^4T_1(^4P)$ excited states (T_d symmetry notations) are possible. From these transitions, only the second and third ones could be detected, as the 10Dq transition, $^4A_2(^4F) \rightarrow {}^4T_2(^4F)$, is shifted to lower energy and usually not detected in tetrahedral complexes of Co^{II}.[32] Distortions related to the presence of two different ligands in the coordination sphere of Co^{II} with roughly axial (C_{3v}) symmetry is manifested in a large splitting of the $^4A_2(^4F) \rightarrow {}^4T_1(^4F)$ transition into two sublevels, ^4E and $^4A_2$, with energies of 6490 and 10820 cm^{-1} above the ground state, respectively. This result is *well-reproduced* by the CASSCF/NEVPT2 calculations (Table 4). The effect of the trigonal field on the magnetic anisotropy will be the subject of the next section.

Theoretical Analysis. *Co(II)−Ligand Bonding As Revealed by a Ligand Field Analysis of the ab Initio Results.* The ligand field parameters, namely, the 5 × 5 ligand field matrix $\mathbf{V}_{LF}$ (eq 6) and the parameter of interelectronic repulsion (B = 965 cm^{-1}), were extracted from a one-to-one mapping procedure as described in Computational Details. The small standard deviation between the ab initio matrix elements and the ones reproduced using the given parameter set (σ = 261 cm^{-1}) shows that the ligand field parametrization is impressively consistent with the CASSCF/NEVPT2 results and may even be used in turn to reproduce such results.

DOI: 10.1021/ja512232f
J. Am. Chem. Soc. 2015, 137, 1993−2005

Table 4. Experimental Vis–NIR Absorption Data for $[Co(Tp^{3\text{-}t\text{-}Bu})N_3]$ and Energies of d–d Transitions from NEVPT2 and CASSCF Calculations

	$^4A_2 \rightarrow {}^4T_1(P)$	$^4A_2 \rightarrow {}^4T_1(F)$	$^4A_2 \rightarrow {}^4T_2(F)$
exptl[a]	14790	6490	not observed
	15020 (sh)	10820	
	15650 (sh)		
	16750 (sh)		
NEVPT2	19773 ($^4A_2$)	6956, 7143 (^4E)	2950, 3154 (^4E)
	20058, 20324 (^4E)	11589 ($^4A_2$)	5749 ($^4A_1$)
CASSCF	21849 ($^4A_2$)	5771, 5888 (^4E)	2649, 2753 (^4E)
	22447, 22625 (^4E)	9307 ($^4A_2$)	4500 ($^4A_1$)

[a]Adopted from ref 1; assignments of band maxima are given according to the irreducible representations of the T_d and C_{3v} (in parenthesis) point groups following this reference and supported by the here reported ab initio computed values.

$$\mathbf{V}_{LF} = \begin{array}{c} \begin{matrix} |d_{xy}\rangle & |d_{yz}\rangle & |d_{z^2}\rangle & |d_{xz}\rangle & |d_{x^2-y^2}\rangle \end{matrix} \\ \begin{bmatrix} -4737 & 1879 & 73 & 245 & -31 \\ 1879 & -6988 & 184 & 16 & 124 \\ 73 & 184 & 562 & 400 & 69 \\ 245 & 16 & 400 & -7319 & -1772 \\ -31 & 124 & 69 & -1772 & -5063 \end{bmatrix} \end{array} \quad (6)$$

Diagonalization of the matrix in eq 6 yields the ligand field orbital energies for complex **1**, which are depicted at the right in Figure 7 (the orbitals are labeled according to the irreducible representations of the C_{3v} point group); the orbital energies for the tetracoordinate complex **2** obtained following the same formalism are plotted at the left in Figure 7. It follows from this comparison that the presence of the fifth (tertiary amine) ligand in **1** leads to a significant shift of the d_{z^2}-type MO to higher energies accompanied by a decrease in the energy separation between the two e-type orbitals.

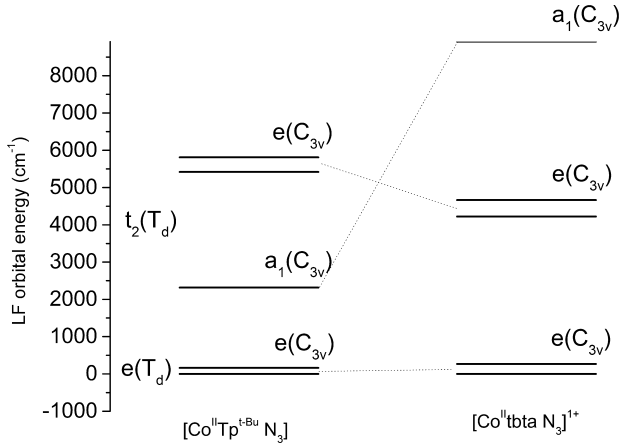

Figure 7. Ab initio ligand field orbital level scheme from a mapping of NEVPT2 energies to ligand field theory for (left) $[Co^{II}(Tp^{3\text{-}t\text{-}Bu})N_3]$ (pseudotetrahedral) and (right) $[Co^{II}(tbta)N_3]^+$ (pseudo-trigonal-bipyramidal) with geometries from X-ray structures.

More insight into the metal–ligand bonding was obtained by angular overlap model analysis of the ligand field matrix $\mathbf{V}_{LF}$. Three different sets of parameters accounting for the difference in the N-donor characters of the ligands in the coordination sphere of Co^{II} are introduced and visualized in Figure 8. These

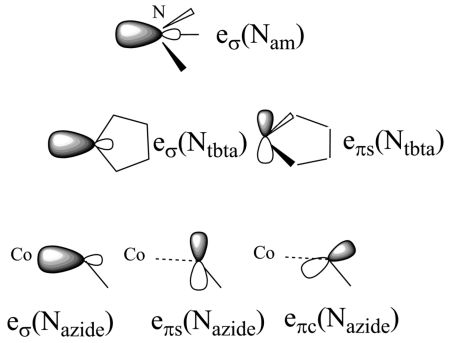

Figure 8. Donor orbital topology of the ligands in the coordination sphere of **1**.

are σ-antibonding parameters for the tertiary amine nitrogen, the tbta nitrogens, and the azide nitrogen [$e_\sigma(N_{amine})$, $e_\sigma(N_{tbta})$, and $e_\sigma(N_{azide})$, respectively]; the Co–N–N_{tbta} and Co–N–N_{azide} out-of-plane π-antibonding parameters [$e_{\pi s}(N_{tbta})$ and $e_{\pi s}(N_{azide})$, respectively]; and finally, one more Co–N–N_{azide} in-plane parameter [$e_{\pi c}(N_{azide})$]. In these considerations, interactions between the metal 3d orbitals and the ligand orbitals involved in strong bonds within the ligand, i.e., the π interactions for N_{amine} and in-plane π interactions for N_{tbta} were neglected. One should note here that with six antibonding parameters, the ligand field matrix $\mathbf{V}_{LF}$ becomes largely overparametrized; parameter covariance prohibits getting all these parameters from a best fit to the matrix elements of eq 6. A prerequisite to apply the AOM is the assumption of the additivity of contributions from different ligands to $\mathbf{V}_{LF}$. We therefore computed $\mathbf{V}_{LF}$ for the $[Co^{II}(tbta)]^{2+}$ fragment without the N_3^- ligand, allowing the set of parameters $e_\sigma(N_{amine})$, $e_\sigma(N_{tbta})$, and $e_{\pi s}(N_{tbta})$ to be derived. We then deduced the ligand field matrix for the N_3^- ligand, $\mathbf{V}_{LF}(N_3)$, from the difference between $\mathbf{V}_{LF}$ for **1** (eq 6)[33] and that for $[Co^{II}(tbta)]^{2+}$, $\mathbf{V}'_{LF}$:

$$\mathbf{V}_{LF}(N_3) = \mathbf{V}_{LF} - \mathbf{V}'_{LF} = \begin{bmatrix} 71 & 250 & 36 & -5 & -17 \\ 250 & 2423 & 194 & 8 & -61 \\ 36 & 194 & 6175 & 396 & 43 \\ -5 & 8 & 396 & 2198 & -68 \\ -17 & -61 & 43 & -68 & -71 \end{bmatrix} \quad (7)$$

In the adopted Cartesian frame, the Co–N_{azide} bond direction coincides with the z axis, the d_{xz} and d_{yz} orbitals are properly oriented for in- and out-of-plane π interactions, and the $d_{x^2-y^2}$ and d_{xy} orbitals are nonbonding and taken as the energy reference. The diagonal matrix elements in eq 7 allow the N_3^- ligand to be uniquely assigned as both a strong σ donor [$e_\sigma(N_{azide}) = 6175\ cm^{-1}$] and π donor [$e_{\pi s}(N_{azide}) = 2423\ cm^{-1}$ and $e_{\pi c}(N_{azide}) = 2198\ cm^{-1}$]. On the basis of the very close values of $e_{\pi s}(N_{azide})$ and $e_{\pi c}(N_{azide})$, N_3^- can be further characterized as a pseudolinear ligand with (because of the bent Co^{II}–N_3 coordination mode) a slight dominance of the out-of-plane π interaction [$e_{\pi s}(N_{azide}) = 2423\ cm^{-1}$] over the in-plane π interaction [$e_{\pi c}(N_{azide}) = 2198\ cm^{-1}$]. The comparison between the values of the parameters for the three ligands shows that the σ-donor character decreases in going from N_3^- to tbta to the tertiary amine. On the basis of the values of e_π, one can infer on the other hand that N_3^- is a stronger π donor than tbta. σ-antibonding energies $e_\sigma(N_{amine})$ = 2802 and

DOI: 10.1021/ja512232f
J. Am. Chem. Soc. 2015, 137, 1993–2005

Table 5. Metal−Ligand Bonding Energies (in cm^{-1}) As Derived from Best Fits of the Angular Overlap Parameters[a] for the Different Ligands of $[Co^{II}(tbta)N_3]^+$ and $[Co^{II}(Tp)N_3]$ to CASSCF and NEVPT2 ab Initio-Derived Ligand Field Matrices

		$[Co^{II}(tbta)N_3]^+$		
structure	method	$e_\sigma(N_{amine})$	$e_\sigma(N_{tbta})$, $e_{\pi s}(N_{tbta})$	$e_\sigma(N_{azide})$, $e_{\pi s}(N_{azide})$, $e_{\pi c}(N_{azide})$
X-ray (SMM)	CASSCF	2255	3664, 1268	6121, 2408, 2195
	CASSCF+NEVPT2	3223	4169, 1404	6193, 2437, 2018, **7121**,[b] **2802**,[b] **2254**[b]
DFT-optimized	CASSCF	1308	3967, 1089	6556, 2788, 2248
	CASSCF+NEVPT2	2068	4455, 1160	6615, 2767, 2113
		$[Co(Tp^{3\text{-t-Bu}})N_3]$		
structure	method	$e_\sigma(N_{amine})$	$e_\sigma(N_{Tp})$, $e_{\pi s}(N_{Tp})$	$e_\sigma(N_{azide})$, $e_{\pi s}(N_{azide})$, $e_{\pi c}(N_{azide})$
X-ray	CASSCF+NEVPT2	−	5132, 1966	5466, 2703, 2675

[a]The notations $e_\sigma(N_{amine})$, $e_\sigma(N_{tbta/Tp})$, and $e_\sigma(N_{azide})$ and $e_{\pi s}(N_{tbta/Tp})$, $e_{\pi s}(N_{azide})$, and $e_{\pi c}(N_{azide})$ refer to the energies of Co−N_{amine}, Co−$N_{tbta/Tp}$, and Co−N_{azide} σ interactions and out-of-plane (πs) and in-plane (πc, for Co−N_{azide}) Co−ligand π interactions, respectively. [b]Numbers in boldface type were derived from the listed NEVPT2 values (6193, 2437, and 2018 cm^{-1}) by multiplying by a factor of 1.15 to adjust the static magnetic data and were used to construct the plots in Figure S4 in the Supporting Information.

Table 6. Parameters of the Effective Spin Hamiltonian (D in cm^{-1}, Equation 5) and Main g-Tensor Values of the (Spin−Orbit) Ground-State Kramers Doublet ($g_{GKD,i}$) from CASSCF and NEVPT2 Calculations on $[Co^{II}(tbta)N_3]^+$ and Complexes with Geometries from X-ray Data and from a DFT Geometry Optimization

	CASSCF				NEVPT2						
	parameters of H_{eff}				parameters of H_{eff}				experimental		
	g_i	D	E/D	$g_{GKD,i}$	g_i	D	E/D	$g_{GKD,i}$	g	D	E/D
X-ray (SMM) $[Co^{II}(tbta)N_3]^+$	2.223	−6.23	0.055	0.357	2.177	−3.93	0.069	0.434	2.34[c]	−10.7[c]	0.22[c]
	2.231			0.379	2.183			0.467			
	2.308			6.913	2.233			6.676			
X-ray (SMM) $[Co^{II}(tbta)]^{2+}$ [a]	2.152	22.86	0.012	2.143	2.124	17.24	0.011	2.120			
	2.387			4.689	2.283			4.492			
	2.393			4.875	2.288			4.492			
DFT-optimized[b] $[Co^{II}(tbta)N_3]^+$	2.213	−6.05	0.105	0.648	2.167	−4.20	0.136	0.802			
	2.227			0.728	2.179			0.924			
	2.295			6.820	2.226			6.567			
X-ray $[Co(Tp^{3\text{-t-Bu}})N_3]$	2.295	5.880	0.134	2.187	2.236	6.962	0.048	2.228	2.02[d]	7.46[d]	0.21[d]
	2.353			3.716	2.321			4.300	2.31[d]		
	2.368			5.613	2.324			4.980	2.48[d]		
X-ray $[Co(Tp^{3\text{-t-Bu}})]^+$ [a]	1.834	106.57	0.008	2.331	1.656	125.06	0.007	2.415			
	2.893			5.496	2.890			5.433			
	2.909			5.646	2.908			5.572			

[a]Model complexes derived from the structures provided by the X-ray data of $[Co^{II}(tbta)N_3]^+$ and $[Co(Tp^{3\text{-t-Bu}})N_3]$ by removing the N_3^- ligand while leaving the geometries of the $[Co^{II}(tbta)]^{2+}$ and $[Co(Tp^{3\text{-t-Bu}})]^+$ fragments unchanged. [b]BP86 exchange−correlation functional and def2-TZVP basis set; 10 van der Waals corrections for nonbonding interactions (following Grimme[22]); COSMO(water) polarizable solvent continuum for charge compensation. [c]Obtained from a fit to the magnetization data from this study (see Static and Dynamic Magnetic Properties). [d]Obtained from high-field EPR data (ref 1).

$e_\sigma(N_{tbta})$ = 4131 cm^{-1} similar to those in **1** (3223 and 4169 cm^{-1}, respectively; see Table 5) have been reported for $Ni^{II}(tbta)_2^{2+}$, in which out of the three triazol N donors only two coordinate to Ni^{II}, thus supporting the formation a *trans*-$(N_{amine})_2(N_{tbta})_4$ complex.[5c] The Ni−N bond distances for the two ligands are similar to those in **1**, and one can conclude from this comparison that in spite of the different coordination numbers (CNs) and angular geometries, the $e_\sigma(N_{amine})$ and $e_\sigma(N_{tbta})$ parameters are fairly well transferrable between the two complexes. This is not surprising since Ni^{II} and Co^{II} are in the same oxidation state and are neighbors in the periodic table. However, for Ni^{II} the orbitals suitable for π bonding (in octahedral complexes t_{2g}:d_{xz},d_{yz},d_{xy}) are fully occupied, and this results in a vanishingly small π-bonding energy of $e_{\pi s}$ = 167 cm^{-1} (compared with $e_{\pi s}$=1404 cm^{-1} for Co^{II}, where orbitals of such type are singly occupied).[5c]

It is customary to divide the contributions to the energies e_λ ($\lambda = \sigma, \pi$) into two terms (eq 8):

$$e_\lambda \approx \langle d_\lambda|\hat{h}|d_\lambda\rangle + \sum_\chi \frac{\langle d_\lambda|\hat{h}'|\chi_\lambda\rangle\langle\chi_\lambda|\hat{h}'|d_\lambda\rangle}{\varepsilon_d - \varepsilon_\chi} \quad (8)$$

in which $\hat{h}$ and $\hat{h}'$ are properly defined as one-electron operators (see refs 34−36 for a review and more details). The first-order term, called the static contribution, is ascribed to the direct electrostatic influence of the ligand and can be identified with the electrostatic matrix element in crystal field theory. Within the adopted ab initio computational scheme, we can associate this term with the CASSCF values of e_σ and e_π (Table 5). The second-order term, called the dynamical contribution, is covalent in nature. Within the ab initio computational scheme, we can associate this term with dynamical correlation subject to NEVPT2 corrections to the CASSCF diagonal matrix

DOI: 10.1021/ja512232f
J. Am. Chem. Soc. 2015, 137, 1993−2005

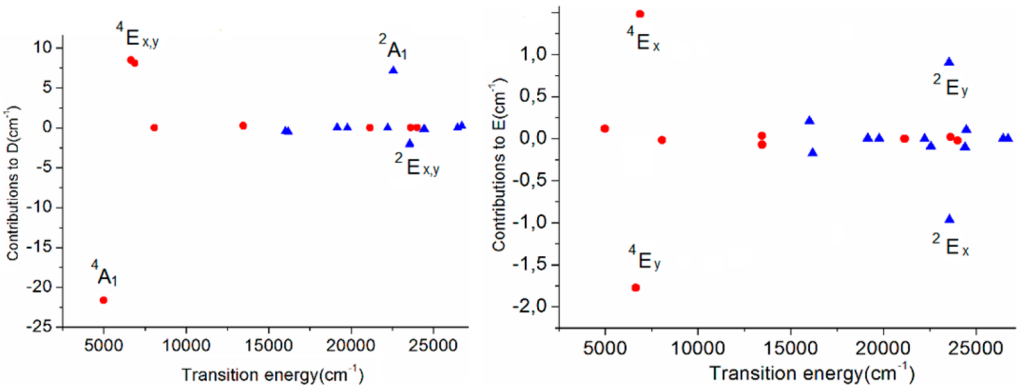

Figure 9. Contributions of excited quartet (red circles) and doublet (blue triangles) states to (left) D and (right) E for complex **1** (X-ray structure, NEVPT2 results).

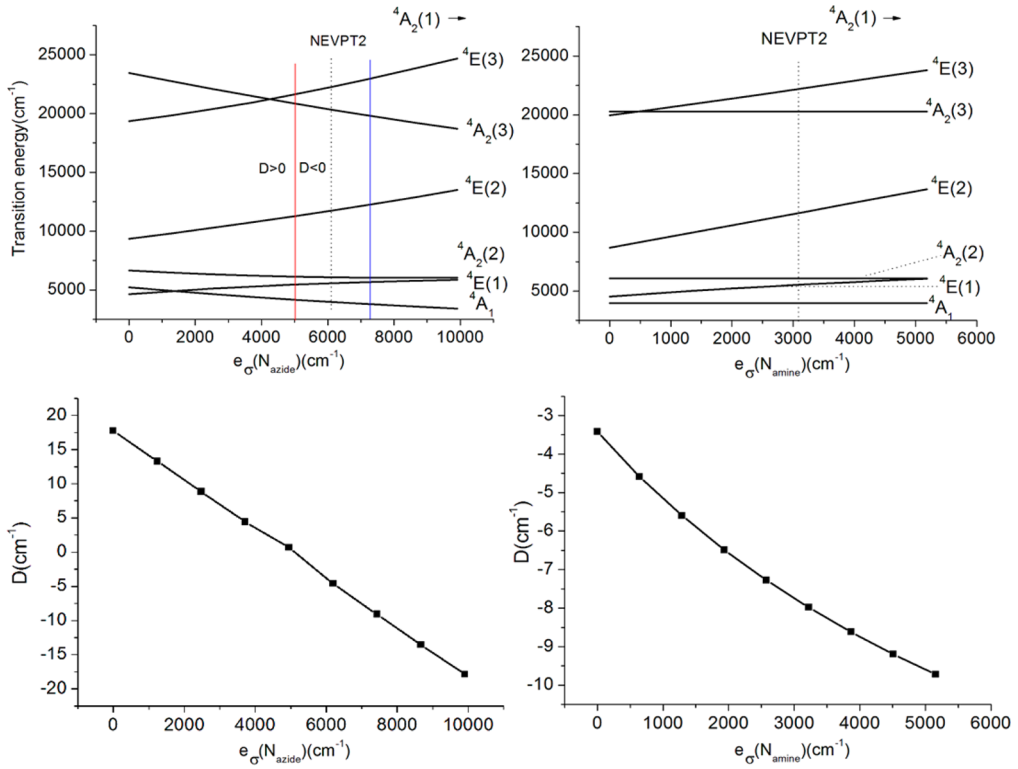

Figure 10. (top) Term energy dependence on the σ-donor strength of the axial ligands in **1** and (bottom) magnetostructural correlation for D as functions of (left) $e_\sigma(N_{azide})$ and (right) $e_\sigma(N_{amine})$. The energy level diagram and D values were computed with reference to a set of ligand field parameters from a one-to-one mapping of NEVPT2 results onto ligand field theory: B = 965 cm^{-1}, C/B = 4.53, $e_\sigma(N_{amine})$ = 3223 cm^{-1}, $e_\sigma(N_{azide})$ = 6193 cm^{-1}, $e_{\pi s}(N_{azide})$ = $e_{\pi c}(N_{azide})$ = 2228 cm^{-1}, $e_\sigma(N_{tbta})$ = 4169 cm^{-1}, $e_{\pi s}(N_{tbta})$ = 1404 cm^{-1}; ζ_{eff} = 515 cm^{-1}. The point-group symmetry was restricted to C_{3v}. The off-linearity of N_3^- was neglected by taking an average over the two parameters $e_{\pi s}(N_{azide})$ = 2437 cm^{-1} and $e_{\pi c}(N_{azide})$ = 2018 cm^{-1}. In plotting the data for N_3^-, the reference value for $e_\sigma(N_{azide})$ was varied while keeping the $e_{\pi s}(N_{azide})/e_\sigma(N_{azide})$ and $e_{\pi c}(N_{azide})/e_\sigma(N_{azide})$ ratios constant at 0.36. The values of the adapted angles were (left) $\angle N_{amine}$–Co–N_{tbta} = 75° and (right) $\angle N_{azide}$–Co–N_{tbta} = 105°. The red vertical line shows the value of $e_\sigma(N_{azide})$ corresponding to a change in the sign of D. The blue vertical line indicates the value of $e_\sigma(N_{azide})$ that reproduces the experimental D value.

elements. It follows that the effect of dynamical correlation for the N-donor ligands increases with decreasing donor character, being the largest for N_{amine} followed by N_{tbta} and N_{azide}. Surprisingly, the e_σ and e_π parameters for N_3^- are not sensitive to such corrections.

Finally, comparison of the Co–N bonding parameters for complexes **1** and **2** shows that the Co–N σ and π interactions for the pyrazolyl N donors of Tp-t-Bu in **2** are considerably stronger than the corresponding ones for tbta in **1**. It is noteworthy that this correlates with opposite trend for Co–N_{azide} σ interactions, which weaken (by 10%) in going from **1** to **2** [it should be noticed that this follows the opposite trend of the Co–N_{azide} bond distance, which gets shorter when the coordination number is lowered from 5 in **1** (Co–N_{azide} = 1.964 Å) to 4 in **2** (Co–N_{azide} 1.919 Å)].

Magnetic Anisotropy and Magnetostructural Correlations in the Light of the ab Initio-Based Ligand Field Analysis. *Qualitative Considerations.* Values of the ZFS parameters D and E and main g-tensor values from CASSCF/NEVPT2 calculations of complexes **1** and **2** in their

DOI: 10.1021/ja512232f
J. Am. Chem. Soc. 2015, 137, 1993–2005

Table 7. Sets of Bonding Parameters $e_\sigma(N_{tbta})$, $e_\sigma(N_{azide})$, and B Resulting from a Direct Fit to Available Spectroscopic Data (d–d Transitions) and from One-to-One Mapping of Quartet Energy Matrices from NEVPT2 to Ligand Field Theory[a,b]

term/parameter	experiment	AOM/direct fit[a]	NEVPT2/mapping
$^4A_2(1) \rightarrow {}^4A_1$	5430	4659 (−771)	4986 (−444)
$^4A_2(1) \rightarrow {}^4E(1)$	6395	6227 (−118)	6649, 6877 (368)
$^4A_2(1) \rightarrow {}^4A_2(2)$	7740	7377 (−363)	8064 (324)
$^4A_2(1) \rightarrow {}^4E(2)$	11960	12900 (940)	13457, 13466 (1502)
$^4A_2(1) \rightarrow {}^4A_2(3)$	15665	16078 (412)	21140 (5475)
$^4A_2(1) \rightarrow {}^4E(3)$	19940	19400 (−540)	23615, 24002 (3868)
$e_\sigma(N_{tbta})$	–	4861	4169
$e_\sigma(N_{azide})$	–	7690	6193
B	–	628	965
standard deviation	–	590	3086

[a]The values of $e_\sigma(N_{amine})$ and the $e_{\pi s}(N_{tbta})/e_\sigma(N_{tbta})$, $e_{\pi s}(N_{azide})/e_\sigma(N_{azide})$, and $e_{\pi c}(N_{azide})/e_\sigma(N_{azide})$ ratios were fixed at 3223 cm^{-1} and 0.334, 0.394, and 0.326, respectively, as given by the NEVPT2 results (see Table 5). [b]Differences between the computed and experimental values are listed in parenthesis.

nonrelativistic $^4A_2$ ground states are listed in Table 6. Without a magnetic field, spin–orbit coupling and the trigonal ligand field induce splitting of the $S = {}^3/_2$ spin state into two Kramers doublets, $M_S = \pm{}^3/_2$ and $M_S = \pm{}^1/_2$, with an energy difference $E(M_S = \pm{}^3/_2) - E(M_S = \pm{}^1/_2)$ equal to twice the ZFS parameter D (eq 5); $E(M_S = \pm{}^3/_2) < E(M_S = \pm{}^1/_2)$ then implies a negative D (easy axis anisotropy) and $E(M_S = \pm{}^3/_2) > E(M_S = \pm{}^1/_2)$ implies a positive D (easy plane anisotropy). In addition to the axial field, orthorhombic distortions (see the structural data in Table 1) induce mixing of the $M_S = \pm{}^3/_2$ and $M_S = \mp {}^1/_2$ magnetic sublevels, and this results in quite significant nonzero values of the parameter E (Table 6 and eq 5). In agreement with experiment, the D value computed by CASSCF/NEVPT2 is negative (positive) in complex **1** (**2**), but quantitatively, the computed values of D and E are in favor of **2**. This will be discussed below. Effective Hamiltonian theory[37] allows one to quantify contributions to these parameters from all excited states spanned by the Co^{II} configuration, the nine quartet ($S = {}^3/_2$) and 40 doublet ($S = {}^1/_2$) states. It follows from these results (Figure 9) that the largest effects on D and E arise from the lowest $^4A_1$ and $^4E(1)$ excited states, which lead to stabilization of the $M_S = \pm{}^3/_2$ and $M_S = \pm{}^1/_2$ levels, respectively, resulting in a negative total D and E. Smaller yet important contributions with an opposite sign for D and E (both positive) originate from the lowest $^2A_1$ and second excited state $^2E(2)$ (Figure 9). The latter are neglected by coupled perturbed Kohn–Sham methods, and indeed, the DFT values of D deviate abnormally from the experimental ones, being also of the wrong sign in the case of **2** (see Table S4 in the Supporting Information). For a tetrahedral (T_d) complex and focusing on the effect of the $^4T_2$ excited state split by trigonal symmetry into $^4A_1$ and $^4E(1)$, second-order perturbation theory yields following expressions for the g-tensor components (eq 9) and the ZFS parameters D (eq 10.1) and E (eq 10.2):

$$g_{zz} = g_e - \frac{8}{3}\frac{\zeta_{eff}}{\Delta(^4T_2^z)}$$

$$g_{xx} = g_e - \frac{8}{3}\frac{\zeta_{eff}}{\Delta(^4T_2^x)} \qquad (9)$$

$$g_{yy} = g_e - \frac{8}{3}\frac{\zeta_{eff}}{\Delta(^4T_2^y)}$$

$$D(^4T_2) = \frac{4\zeta_{eff}^2}{9}\left[\frac{1}{2}\left(\frac{1}{\Delta(^4E_x(1))} + \frac{1}{\Delta(^4E_y(1))}\right) - \frac{1}{\Delta(^4A_1)}\right] \qquad (10.1)$$

$$E(^4T_2) = \frac{2\zeta_{eff}^2}{9}\left[\frac{1}{\Delta(^4E_y(1))} - \frac{1}{\Delta(^4E_x(1))}\right] \qquad (10.2)$$

in which ζ_{eff} is the effective spin–orbit coupling parameter of Co^{II} and $\Delta(^4A_1)$, $\Delta(^4E_x(1))$, and $\Delta(^4E_y(1))$ are the energies of electronic transitions from the nonrelativistic $^4A_2$ ground state into the $^4A_1$ and $^4E(1)$ [$^4E_x(1)$, $^4E_y(1)$] excited states (the notation follows C_{3v} point-group symmetry). The sign and magnitude of the energy separation between $^4A_1$ and $^4E(1)$, which according to eq 10.1 determines D, can be tuned by changing the nature of the axial ligands and/or simply by imposing structural changes leading to variations of the metal–ligand bond distances. Using $e_\sigma(N_{amine})$ and $e_\sigma(N_{azide})$ as chemical/structural variables [and adopting values of $e_{\pi s}(N_{azide})/e_\sigma(N_{azide})$, $e_{\pi c}(N_{azide})/e_\sigma(N_{azide})$, and all other parameters according to the AILFT-NEVPT2 results], we explore in Figure 10 the effect of the Lewis basicity on the term energies and D. Values of zero for $e_\sigma(N_{azide})$ (Figure 10, left) and $e_\sigma(N_{amine})$ (Figure 10, right) correspond to four-coordinate trigonal complexes with two different axial ligands of different natures: the *σ-only* modest type of N donor due to the tertiary amine (left) and the *both σ- and π-type* stronger N donor due to N_3^- (right). The different Lewis basicities of the two N donors and the correspondingly different angular geometries [$\angle N_{amine}$–Co–N_{tbta} = 75° (left), $\angle N_{azide}$–Co–N_{tbta} = 105° (right)] lead to a switch in the level ordering from $^4E(1) < {}^4A_1$ (Figure 10, top left) to $^4A_1 < {}^4E(1)$ (Figure 10, top right), and this correlates with the change in the value of D from large and positive (Figure 10, bottom left) to modest and negative (Figure 10, bottom right), in agreement with eq 10.1. In contrast to the σ-only tertiary amine N donor, for which the energy of $^4A_2(1) \rightarrow {}^4A_1$ [and $^4A_2(1) \rightarrow {}^4A_2(2)$ and $^4A_2(1) \rightarrow {}^4A_2(3)$ as well] is strictly independent of $e_\sigma(N_{amine})$, the Co–N σ and π interactions lead to a decrease in this energy with increasing $e_\sigma(N_{azide})$ [where, because of the fixed values of $e_{\pi s}(N_{azide})/e_\sigma(N_{azide})$ and $e_{\pi c}(N_{azide})/e_\sigma(N_{azide})$, the values of $e_{\pi s}(N_{azide})$ and $e_{\pi c}(N_{azide})$ also increase]. Since $^4A_2(1) \rightarrow {}^4E(1)$

DOI: 10.1021/ja512232f
J. Am. Chem. Soc. 2015, 137, 1993–2005

is affected by this, changes in the opposite direction, namely, a switch in the level ordering from $^4E(1) < {}^4A_1$ to $^4A_1 < {}^4E(1)$, takes place already at the moderate value of $e_\sigma(N_{azide}) = 1750$ cm^{-1}. This results in a change in D from large and positive to large and negative with increasing Lewis basicity $[e_\sigma(N_{azide})]$. However, low-symmetry distortions (observed in the X-ray structure of **1**) become energetically amplified with increasing Lewis basicity $[e_\sigma(N_{azide})]$ and induce a larger transverse anisotropy (larger E; Figure S1 in the Supporting Information). In contrast to azide-like ligands, variation of $e_\sigma(N_{amine})$ does not lead to crossing of the $^4E(1)$ and $^4A_1$ levels; with $^4A_1 < {}^4E(1)$, D remains accordingly negative in sign and modest in magnitude (Figure 10, bottom right).

Quantitative Comparison with Experiment. One-to-one mapping of ligand field theory to CASSCF and NEVPT2 calculations allows numerical results from ab initio calculations to be translated into chemical language and therefore to assist with predictions. In the preceding section, Co−N bonding parameters extracted in such a way have been used to derive magnetostructural correlations and thus to relate the magnetic anisotropy (quantified by D and E) with variations in structure and bonding. Multireference electronic structure calculations going beyond CASSCF/NEVPT2 are moreover subject to further developments and improvements, and it might be interesting here to compare the ligand field parameters deduced from mapping to such calculations with their values derived from a *direct fit* to experimental spectroscopic and magnetic data. The rich d−d absorption spectrum (Figure 6 and Tables 2 and 3) is excellent for such a purpose. In Table 7, the AOM parameters $e_\sigma(N_{tbta})$, $e_\sigma(N_{azide})$, and B derived from the best fit to the energies of the six observed d−d transitions of **1** are compared with values resulting from the mapping to the NEVPT2 (CASSCF) eigenvalues (eigenfunctions). In the former fits, $e_\sigma(N_{amine})$ and the $e_{\pi s}(N_{tbta})/e_\sigma(N_{tbta})$, $e_{\pi s}(N_{azide})/e_\sigma(N_{azide})$, and $e_{\pi c}(N_{azide})/e_\sigma(N_{azide})$ ratios were fixed at their NEVPT2 values of 3223 cm^{-1} and 0.334, 0.394, and 0.326, respectively (Table 5), while $e_\sigma(N_{tbta})$, $e_\sigma(N_{azide})$, and B were readjusted to improve the agreement with experiment.[38] The results show that the $e_\sigma(N_{tbta})$ and $e_\sigma(N_{azide})$ values adjusted to match experiment (4861 and 7690 cm^{-1}, respectively; Table 7) are slightly larger (by 16% and 24%, respectively) than the NEVPT2 values (4169 and 6193 cm^{-1}; Table 5). In contrast, a 35% smaller value of B (628 cm^{-1}, compared with the NEVPT2 value of 965 cm^{-1}) was obtained from a direct fit to experiment. Apparently, more efforts at the ab initio level of theory are needed in order to better account for the nephelauxetic effect. A closer look at the energy dependence of the quartet energy levels on B (Figure S2 in the Supporting Information) shows that the energies of spin-allowed transitions are not equally affected by B. Thus, while the energies of the lowest three observed transitions were well-reproduced by NEVPT2 (within error bars between −444 and 368 cm^{-1}), a larger deviation (1502 cm^{-1}) was found for the 12000 cm^{-1} transition and even bigger ones (5475 and 3868 cm^{-1}) were observed for the two topmost energy levels (observed at 15700 and 20000 cm^{-1}, respectively). As was discussed before, the deviations between computed theoretical and experimental energies of d−d transitions are due to the effect of excited charge transfer states, which becomes increasingly pronounced when closing the energy between charge transfer and 3d^n multiplets. This discrepancy presents a challenge for multireference electronic structure theories. To this end, a more detailed account of dynamical correlations is needed. As pointed out above, this problem is only partly cured by going to larger active spaces.

It follows from Table 7 that low-lying electronic states are well-reproduced by NEVPT2/CASSCF, and this explains the overall success of these methods for the interpretation and prediction of the magnetic anisotropy in spin centers with open 3d shells. However, the computed values of D and E for **1** (Table 6) are distinctly lower than those extracted from the magnetic data. In line with this, we found some deviations between the computed and experimental magnetic susceptibilities (χT) and magnetizations (M) (Figure S3 in the Supporting Information). However, an increase in the parameters $e_\sigma(N_{azide})$, $e_{\pi s}(N_{azide})$, and $e_{\pi c}(N_{azide})$ by only 15% greatly improves the agreement between theory and experiment (Figure S3 in comparison with Figure S4 in the Supporting Information). This shows the sensitivity of the magnetic anisotropy to subtle changes in structure and bonding (also see the discussion in ref 7).

■ CONCLUSIONS

(1) The novel complex $[Co^{II}(tbta)N_3]^+$ (**1**) (tbta = tris[(1-benzyl-1*H*-1,2,3-triazol-4-yl)methyl]amine) has been characterized experimentally (magnetically and by d−d absorption spectroscopy) and theoretically (by means of multireference electronic structure calculations). The complex displays slow relaxation of the magnetization in an applied external magnetic field of H = 3000 Oe and easy-axis anisotropy (D = −10.7 cm^{-1}) superimposed with a quite significant orthorhombic anisotropy (E/D = 0.22). The latter is a possible cause for the absence of any maximum in the frequency dependence of the imaginary part of the ac susceptibility in zero field.

(2) By means of N-electron valence second-order perturbation theory (NEVPT2), low-lying experimentally observed d−d transitions could be nicely reproduced. Ligand field parameters were derived from a one-to-one mapping of ligand field theory onto the ab initio wave functions and energy eigenvalues. On the basis of these parameters, the N donors coordinating to Co^{II} were characterized as weak in the case of the tertiary amine nitrogen, stronger for the triazole nitrogens, and, contrary to previous results,[1] strong for the azido ligand.

(3) Magnetostructural correlations show a strong increase/decrease in the negative D/E values with increasing Lewis basicity (decreasing Co−N bond distance) of the considered axial ligand trans to the tertiary amine nitrogen. The effect on the change in the sign of D in going from four-coordinate Co^{II} (positive D) to five-coordinate Co^{II} (negative D) has been discussed, and it has been shown that the magnetic anisotropy quantified by the parameters D and E is extremely sensitive to subtle changes in structure and bonding.

(4) Even though the literature contains some examples of mononuclear Co(II) complexes displaying slow relaxation of the magnetization,[39] the present work is the first time that the "magnetically ubiquitous" azido ligand has been used in combination with Co(II) for this purpose. Furthermore, it is a rare occasion where insights into bonding and magnetic anisotropy from experiment and theory have been utilized to describe slow relaxation of the magnetization in these systems and to gain information about the sign of D. In doing so, we have provided valuable details concerning the ligand field nature of the azido ligand and obtained correlations between structure, bonding parameters, and magnetic anisotropy for these systems.

DOI: 10.1021/ja512232f
J. Am. Chem. Soc. 2015, 137, 1993−2005

(5) Finally, some comments about the quantitative aspects of the ab initio theory employed in this study are due. While ab initio methods are in principle exact, their practical realization (implementation) involves a series of approximations. As a post-Hartree−Fock-based method, the CASSCF wave function is too ionic; this leads to underestimation of quantities related to metal−ligand covalence, such as nephelauxetic reduction of the parameters of interelectronic repulsion B and C and oscillator strengths, and gives computed d−d transition energies that are too large compared with the experimentally reported ones. Partial inclusion of ligand-to-metal charge transfer via second-order perturbation theory (NEVPT2) improves the metal−ligand covalence and shifts the high-energy d−d transitions in the right direction. By means of a one-to-one mapping of ligand field theory onto ab initio energy eigenvalues and eigenfunctions, important contributions of dynamical correlation to the energy parameters quantifying the metal−ligand bonding of the tbta and amine N donors have been deduced, while the azide N donor was found to be less affected by such influences. However, as a result of error compensation, the D values computed using CASSCF are superior to the NEVPT2 ones. By comparison, it was also shown that for the complexes in this study, DFT is of very limited use (see the recent review in ref 40 for more details).

■ ASSOCIATED CONTENT

Supporting Information

Tables containing experimental crystallographic details for **1** and a comparison of ligand field orbital energies obtained from experimental and calculated structures; figures showing the variation of E with σ-donor strength of the axial ligand, term energies as functions of B, and the field dependence of the magnetic susceptibility together with calculated values; and coordinates from geometry optimization. This material is available free of charge via the Internet at http://pubs.acs.org.

■ AUTHOR INFORMATION

Corresponding Authors

*mihail.atanasov@cec.mpg.de
*frank.neese@cec.mpg.de
*Biprajit.sarkar@fu-berlin.de

Author Contributions

⊥D.S. and M.G.S. contributed equally.

Notes

The authors declare no competing financial interest.

■ ACKNOWLEDGMENTS

We are grateful to the Fonds der Chemischen Industrie for financial support of this work (Chemiefonds Stipendium for M.G.S.).

■ REFERENCES

(1) Krzystek, J.; Swenson, D. C.; Zvyagin, S. A.; Smirnov, D.; Ozarowski, A.; Telser, J. *J. Am. Chem. Soc.* **2010**, *132*, 5241.

(2) Feng, P. L.; Koo, C.; Henderson, J. J.; Manning, P.; Nakano, M.; del Barco, E.; Hill, S.; Hendrickson, D. N. *Inorg. Chem.* **2009**, *48*, 3480.

(3) For selected reviews, see: (a) Ribas, J.; Escuer, A.; Monfort, M.; Vincente, R.; Cortés, R.; Lezama, L.; Rojo, T. *Coord. Chem. Rev.* **1999**, *193−195*, 1027. (b) Escuer, A.; Aromi, G. *Eur. J. Inorg. Chem.* **2006**, 4721. (c) Lin, X.-J.; Shen, Z.; Song, Y.; Xu, H.-J.; Li, Y.-Z.; You, X.-Z. *Inorg. Chim. Acta* **2005**, *358*, 1963. (d) Mukherjee, S.; Mukherjee, P. S. *Acc. Chem. Res.* **2013**, *46*, 2556. (e) Zheng, Y.-F.; Hu, X.; Liu, F.-C.; Bu, X.-H. *Chem. Soc. Rev.* **2009**, *38*, 469. (f) Escuer, A.; Esteban, J.; Perlepes, S. P.; Stamatatos, T. C. *Coord. Chem. Rev.* **2014**, *275*, 87. (g) Wang, X.-Y.; Wang, Z.-M.; Gao, S. *Chem. Commun.* **2008**, 281. (h) Adhikary, C.; Koner, S. *Coord. Chem. Rev.* **2010**, *254*, 2933.

(4) (a) Struthers, H.; Mindt, T. L.; Schibli, R. *Dalton Trans.* **2010**, *39*, 675. (b) Crowley, J. D.; McMorran, D. *Top. Heterocycl. Chem.* **2012**, *22*, 31. (c) Schweinfurth, D.; Deibel, D.; Weisser, F.; Sarkar, B. *Nachr. Chem.* **2011**, *59*, 937. (d) Schulze, B.; Schubert, U. S. *Chem. Soc. Rev.* **2014**, *43*, 2522.

(5) (a) Schweinfurth, D.; Weisser, F.; Bubrin, D.; Bogani, L.; Sarkar, B. *Inorg. Chem.* **2011**, *50*, 6114. (b) Schweinfurth, D.; Demeshko, S.; Khusniyarov, M. M.; Dechert, S.; Gurram, V.; Buchmeiser, M. R.; Meyer, F.; Sarkar, B. *Inorg. Chem.* **2012**, *51*, 7592. (c) Schweinfurth, D.; Krzystek, J.; Schapiro, I.; Demeshko, S.; Klein, J.; Telser, J.; Ozarowski, A.; Su, C.-Y.; Meyer, F.; Atanasov, M.; Neese, F.; Sarkar, B. *Inorg. Chem.* **2013**, *52*, 6880. (d) Schweinfurth, D.; Klein, J.; Hohloch, S.; Dechert, S.; Demeshko, S.; Meyer, F.; Sarkar, B. *Dalton Trans.* **2013**, *42*, 6944. (e) Donnelly, P. S.; Zanatta, S. D.; Zammit, S. C.; White, J. M.; Williams, S. J. *Chem. Commun.* **2008**, 2459. (f) Schweinfurth, D.; Demeshko, S.; Hohloch, S.; Steinmetz, M.; Brandenburg, J. G.; Dechert, S.; Meyer, F.; Grimme, S.; Sarkar, B. *Inorg. Chem.* **2014**, *53*, 8203. (g) Weisser, F.; Hohloch, S.; Plebst, S.; Schweinfurth, D.; Sarkar, B. *Chem.—Eur. J.* **2014**, *20*, 781. (h) Connell, T. U.; Schieber, C.; Silvestri, I. P.; White, J. M.; Williams, S. P.; Donnelly, P. S. *Inorg. Chem.* **2014**, *53*, 6503.

(6) Atanasov, M.; Ganyushin, D.; Sivalingam, K.; Neese, F. *Struct. Bonding (Berlin)* **2012**, *143*, 149.

(7) Atanasov, M.; Ganyushin, D.; Pantazis, D. A.; Sivalingam, K.; Neese, F. *Inorg. Chem.* **2011**, *50*, 7640.

(8) Atanasov, M.; Zadrozny, J. M.; Long, J. R.; Neese, F. *Chem. Sci.* **2013**, *4*, 139.

(9) Hein, J. E.; Krasnova, L. B.; Iwasaki, M.; Fokin, V. V. *Org. Synth.* **2011**, *88*, 238.

(10) Malmqvist, P.-Å; Roos, B. O. *Chem. Phys. Lett.* **1989**, *155*, 189.

(11) Angeli, C.; Cimiraglia, R.; Malrieu, J.-P. *Chem. Phys. Lett.* **2001**, *350*, 297.

(12) Angeli, C.; Cimiraglia, R.; Evangelisti, S.; Leininger, T.; Malrieu, J.-P. *J. Chem. Phys.* **2001**, *114*, 10252.

(13) Angeli, C.; Cimiraglia, R.; Malrieu, J.-P. *J. Chem. Phys.* **2002**, *117*, 9138.

(14) Borini, S.; Cestari, M.; Cimiraglia, R. J. *J. Chem. Phys.* **2004**, *121*, 4043.

(15) Angeli, C.; Bories, B.; Cavallini, A.; Cimiraglia, R. *J. Chem. Phys.* **2006**, *124*, No. 054108.

(16) Neese, F. *Wiley Interdiscip. Rev.: Comput. Mol. Sci.* **2012**, *2*, 73.

(17) Neese, F.; with contributions from Becker, U.; Ganyushin, D.; Hansen, A.; Izsak, R.; Liakos, D. G.; Kollmar, C; Kossmann, S.; Pantazis, D. A.; Petrenko, T.; Reimann, C.; Riplinger, C.; Roemelt, M.; Sandhöfer, B.; Schapiro, I.; Sivalingam, K.; Wennmohs, F.; Wezisla, B.; and contributions from our collaborators Kállay, M.; Grimme, S.; Valeev, E. *ORCA: An ab Initio, DFT, and Semiempirical SCF-MO Package*, version 3.0; MPI für Chemische Energiekonversion: Mülheim an der Ruhr, Germany. Binaries of ORCA for a variety of platforms are available free of charge for academic users.

(18) Neese, F. *J. Chem. Phys.* **2005**, *122*, No. 034107.

(19) Ganyushin, D.; Neese, F. *J. Chem. Phys.* **2006**, *125*, No. 024103.

(20) Jørgensen, C. K.; Pappalardo, R.; Schmidtke, H.-H. *J. Chem. Phys.* **1963**, *39*, 1422.

(21) Schäffer, C. E.; Jørgensen, C. K. *Mol. Phys.* **1965**, *9*, 401.

(22) (a) Grimme, S.; Anthony, J.; Ehrlich, S.; Krieg, H. *J. Chem. Phys.* **2010**, *132*, No. 154104. (b) Grimme, S.; Ehrlich, S.; Goerigk, L. *J. Comput. Chem.* **2011**, *32*, 1456.

(23) Schäfer, A.; Horn, H.; Ahlrichs, R. *J. Chem. Phys.* **1992**, *97*, 2571.

(24) Weigend, F.; Ahlrichs, R. *Phys. Chem. Chem. Phys.* **2005**, *7*, 3297.

(25) Klamt, A.; Schüürman, G. *J. Chem. Soc., Perkin Trans. 2* **1993**, 799.

(26) Klamt, A. *J. Phys. Chem.* **1996**, *100*, 3349.

(27) Adamsky, H. *AOMX: A FORTRAN Program for the Calculation of d^n terms within the Angular Overlap Model with Interelectronic Repulsion and Spin-Orbit Coupling*; Institute of Theoretical Chemistry,

DOI: 10.1021/ja512232f
J. Am. Chem. Soc. 2015, 137, 1993−2005

Heinrich-Heine-University: Düsseldorf, Germany, 1995. This program, both executable and source code, are freely available at www.aomx.de.
(28) Sheldrick, G. M. *Acta Crystallogr.* **2008**, *A64*, 112.
(29) Kahn, O. *Molecular Magnetism*; VCH: New York, 1993.
(30) Gatteschi, D.; Sessoli, R.; Villain, J. *Molecular Nanomagnets*; Oxford University Press: New York, 2006.
(31) Bertini, I.; Ciampolini, M.; Gatteschi, D. *Inorg. Chem.* **1973**, *12*, 693.
(32) Lever, A. B. P. *Inorganic Electronic Spectroscopy*; Elsevier: Amsterdam, 1984.
(33) In taking the difference, an arbitrary energy shift for the two matrices was eliminated by converting these into a traceless form, i.e., ensuring that the sum of the diagonal elements of each matrix is zero.
(34) Schönherr, T.; Atanasov, M.; Adamsky, H. In *Comprehensive Coordination Chemistry II*; Elsevier: Amsterdam, 2003; Vol. *2*, Chapter 2.36, pp 443−455.
(35) Gerloch, M.; Woolley, R. G. *Prog. Inorg. Chem.* **1984**, *31*, 371.
(36) Bridgeman, A. J.; Gerloch, M. *Prog. Inorg. Chem.* **1997**, *45*, 179.
(37) (a) Maurice, R.; Bastardis, R.; de Graaf, C.; Suaud, N.; Mallah, T.; Guihéry, N. *J. Chem. Theory Comput.* **2009**, *5*, 2977. (b) Maurice, R.; Guihéry, N.; Bastardis, R.; de Graaf, C. *J. Chem. Theory Comput.* **2010**, *6*, 55;Erratum: **2010**, *6*, 977. (c) Maurice, R.; Pradipto, A. M.; Guihéry, N.; Broer, R.; de Graaf, C. *J. Chem. Theory Comput.* **2010**, *6*, 3092. (d) Maurice, R.; de Graaf, C.; Guihéry, N. *J. Chem. Phys.* **2010**, *133*, No. 084307. The formalism developed in these references was implemented and is available in the recent release of ORCA 3.1 (see ref 17).
(38) Because of parameter covariance, no unique fit from spectroscopic data is possible; this problem also arises when the number of variables is larger than the number of observables (overparametrization).
(39) For selected examples, see: (a) Zadrozny, J. M.; Long, J. R. *J. Am. Chem. Soc.* **2011**, *133*, 20732. (b) Raznak, C.; Cremades, E.; Fuhr, O.; Ruben, M.; Boca, R. *Inorg. Chem.* **2014**, *53*, 8200. (c) Boca, R.; Miklovic, J.; Titis, J. *Inorg. Chem.* **2014**, *53*, 2367. (d) Cao, D.-K.; Feng, J.-Q.; Ren, M.; Gu, Y.-W.; Song, Y.; Ward, M. D. *Chem. Commun.* **2013**, *49*, 8863. (e) Eichhöfer, A.; Lan, Y.; Mereacre, V.; Bodenstein, T.; Weigend, F. *Inorg. Chem.* **2014**, *53*, 1962. (f) Zadrozny, J. M.; Liu, J.; Piro, N. A.; Chang, C. J.; Hill, S.; Long, J. R. *Chem. Commun.* **2012**, *48*, 3897. (g) Gomez-Coca, S.; Urtizberea, A.; Cremades, E.; Alonso, P. J.; Camon, A.; Ruiz, E.; Luis, F. *Nat. Commun.* **2014**, *5*, No. 4300. (h) Habib, F.; Luca, O. R.; Vieru, V.; Shiddiq, M.; Korobkov, I.; Gorelksy, S. I.; Takase, M. K.; Chibotaru, L. F.; Hill, S.; Crabtree, R. H.; Murugesu, M. *Angew. Chem., Int. Ed.* **2013**, *52*, 11290. (i) Vallejo, J.; Castro, I.; Ruiz-Garcia, R.; Cano, J.; Julve, M.; Lloret, F.; De Munno, G.; Wernsdorfer, W.; Pardo, E. *J. Am. Chem. Soc.* **2012**, *134*, 15704. (j) Buchholz, A.; Eseola, A. O.; Plass, W. *C. R. Chim.* **2012**, *15*, 929. (k) Jurca, T.; Farghal, A.; Lin, P.-H.; Korobkov, I.; Murugesu, M.; Richeson, D. S. *J. Am. Chem. Soc.* **2011**, *133*, 15814. (l) Chen, L.; Wang, J.; Wei, J.-M.; Wernsdorfer, W.; Chen, X.-T.; Zhang, Y.-Q.; Song, Y.; Xue, Z.-L. *J. Am. Chem. Soc.* **2014**, *136*, 12213. (m) Yang, F.; Zhou, Q.; Zhang, Y.; Zeng, G.; Li, G.; Shi, Z.; Wang, B.; Feng, S. *Chem. Commun.* **2013**, *49*, 5289. (n) Herchel, R.; Vahovska, L.; Potocnak, I.; Travnicek, Z. *Inorg. Chem.* **2014**, *53*, 5896. (o) Gomez-Coca, S.; Cremades, E.; Aliaga-Alcalde, N.; Ruiz, E. *J. Am. Chem. Soc.* **2013**, *135*, 7010. (p) Saber, M. R.; Dunbar, K. R. *Chem. Commun.* **2014**, *50*, 12266.
(40) Atanasov, M.; Aravena, D.; Suturina, E.; Bill, E.; Maganas, D.; Neese, F. *Coord. Chem. Rev.* **2014**, DOI: 10.1016/j.ccr.2014.10.015.

DOI: 10.1021/ja512232f
J. Am. Chem. Soc. 2015, 137, 1993−2005